Cooperative Localization and Tracking using Multipath Channel Information

Josef Kulmer, Erik Leitinger, Paul Meissner, Stefan Hinteregger, and Klaus Witrisal
Graz University of Technology, Austria
email: {kulmer, erik.leitinger, paul.meissner, stefan.hinteregger, witrisal}@tugraz.at

***Abstract*—Indoor environments are characterized by harsh multipath conditions. Multipath-assisted indoor navigation and tracking (MINT) exploits position-related features of the propagation channel to improve its *accuracy* and *robustness*. In this work we introduce an anchor-free, cooperative MINT algorithm. The algorithm uses monostatic and bistatic (cooperative) measurements conducted by the agents. The estimated multipath components are associated to virtual anchors exploiting their position-related information. We present a proof-of-concept using data from an ultra-wideband measurement campaign, reaching a position accuracy better than 6 cm for 90 % of the measurement points.**

I. Introduction

Radio-based position tracking with high levels of *accuracy* and *robustness* has received a lot of attention over the last decades. The achievable performance depends strongly on the environment determining the radio propagation. In indoor environments high levels of accuracy and robustness are hindered by harsh multipath propagation. The undesired multipath can be countered by data fusion of multiple information sources [1] or by providing remedies against the errors induced by the multipath propagation [2].

Another way of tackling this problem is to exploit useful position-related information contained in multipath components (MPCs) [3]. Association of the MPCs to the surrounding geometry enables improved localization performance, as shown in [3]–[7]. The received signal is modeled as a superposition of the line-of-sight component (LOS) and so-called *deterministic* MPCs originating from reflections at objects, e.g. wall segments. These reflections can be used to gain additional information for localization and tracking, which is especially needed in scenarios with a low number of anchor nodes. Localization methods relying on a single-anchor node were presented in [8]–[10].

A low number of anchor nodes reduces the position accuracy and robustness. This can be circumvented by cooperation among the agents as shown in [10]–[15]. In [12] several agents locate their positions using a single anchor by employing a sum-product based message passing algorithm. The method shown in [13] presents cooperative localization of two agents and three anchors using convex optimization. In [14] and [15] cooperative tracking is realized without using any infrastructure but exploiting multipath. The tracking algorithms are realized using the belief propagation scheme SPAWN [11] and an algorithm based on extended Kalman filters, respectively.

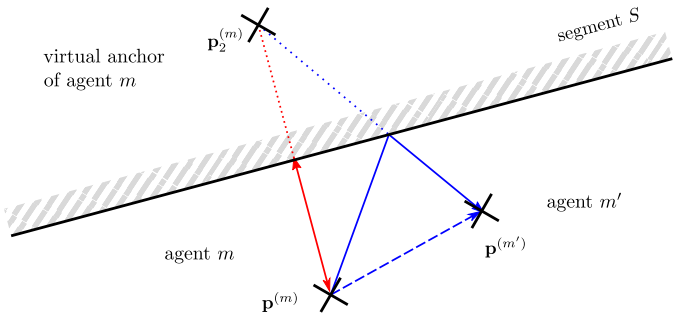

Fig. 1. Multipath propagation of monostatic (red) and bistatic (blue) measurements. The emitted pulse of agent m is received by its neighbor m' (bistatic) and by itself (monostatic) and contains the line-of-sight and a multipath component due to the reflection at wall segment S. Mapping of the reflection to the virtual anchor at position $\mathbf{p}_2^{(m)}$ models the geometry of the multipath component.

In this work we present an anchor-free, cooperative tracking algorithm exploiting multipath propagation as extension to [15] by considering uncertainty of virtual anchors (VAs). We use ultra-wideband (UWB) signals as their superior time resolution enables separation of MPCs. The MPCs can be modeled as signals emitted from virtual anchors. This yields a simple geometric model of the delays of the deterministic MPCs which allows exploiting their position related information as shown in Fig. 1. The agent and corresponding VA positions are tracked with an extended Kalman Filter (EKF) making use of *monostatic* and *bistatic* measurements. To obtain the monostatic measurements, each agent acts as receiver and transmitter whereas the bistatic measurements are performed in between neighboring (cooperating) agents (see Fig. 1). We show the performance of the proposed algorithm for synthetic and real measurement data in terms of accuracy and robustness with respect to imprecise floorplans.

The key contributions of this paper are:

- We formulate the relations between the agent and VA positions, velocities and covariances.
- We present an anchor-free, cooperative algorithm using data association of MPC delays with according VAs and assemble the EKF for tracking the joint state of the agents and the according VAs.
- We show the applicability of the presented algorithm on real data.

The paper is organized as follows: Section II provides an overview about the subject and introduces the geometric-

stochastic signal model and the VA motion model, respectively. Section III describes the implementation of the cooperative algorithm, while Sections IV and V wrap up the paper with results, discussions, and conclusions.

II. Problem Formulation

Several clock-synchronized agents $m \in \mathcal{N}_m = \{1, \dots, M\}$ aim at localizing their positions $\mathbf{p}_n^{(m)}$ at time step n using monostatic and bistatic measurements. The measurements are performed by transmitting UWB signals $s(t)$ which interact with the environment resulting in multipath propagation. We apply a geometrical model for multipath propagation by employing VAs, as illustrated in Fig. 1. In the bistatic measurement setup, the emitted pulse of agent m is received at neighboring agent m' as a sum of an LOS component (dashed blue line) and a reflection (solid blue line) at the wall segment S (solid gray line). We model this reflection as a pulse emitted from VA $\mathbf{p}_2^{(m)}$, whose position is defined by the image-source-model [16]. In the monostatic measurement setup, the pulse is emitted and received by agent m. Again, the reflection at the wall segment (solid red line) is modeled as a pulse emitted from a VA at position $\mathbf{p}_2^{(m)}$. For a better readability, we drop the time step index n.

A. Signal Model

The received signal $r^{(m',m)}(t)$ of agent m' for the emitted pulse $s(t)$ of agent m is modeled according to [3], [17]

$$r^{(m',m)}(t) = \sum_{k=1}^{K^{(m',m)}} \alpha_k^{(m',m)} s\big(t - \tau_k^{(m',m)}\big) + \big(s * \nu^{(m',m)}\big)(t) + w(t), \tag{1}$$

for both monostatic ($m = m'$) and bistatic ($m \neq m'$) measurements. The first term of (1) denotes the sum of deterministic MPCs with complex amplitudes $\alpha_k^{(m',m)}$ and delays $\tau_k^{(m',m)}$, originating from agent m with corresponding VAs at positions $\mathbf{p}_k^{(m)}$. The delays are calculated according to $\tau_k^{(m',m)} = \frac{1}{c}\big\|\mathbf{p}^{(m')} - \mathbf{p}_k^{(m)}\big\|$ with $k \in \big\{1, \dots, K^{(m',m)}\big\}$ and c denoting the speed of light. The number of VAs $K^{(m',m)}$ depends on the agent positions $\mathbf{p}^{(m)}$ and $\mathbf{p}^{(m')}$. The model does not distinguish between the LOS component and reflected MPCs by declaring $\mathbf{p}_1^{(m)} = \mathbf{p}^{(m)}$.

The second term in (1) denotes the convolution of the transmitted signal $s(t)$ and the diffuse multipath (DM) $\nu^{(m',m)}$. The DM is modeled as a realization of a non-stationary, zero-mean Gaussian random process. We assume uncorrelated scattering along τ, resulting in an auto-correlation function of $K_\nu^{(m',m)}(\tau, u) = \mathbb{E}_\nu\big\{\nu^{(m',m)}(\tau)\nu^{(m',m)*}(u)\big\} = S_\nu^{(m',m)}(\tau)\delta(\tau - u)$ with $S_\nu^{(m',m)}(\tau)$ denoting the power delay profile (PDP) of the diffuse multipath. According to [18], the PDP depends on the position of transmitter and receiver and is quasi-stationary in the spatial domain. Note, that the DM comprises all other not modeled, dense MPCs and represents a interference to the useful deterministic MPCs.

The last term denotes additive white Gaussian noise with a double-sided power spectral density (PSD) of $N_0/2$.

B. Virtual Anchor Motion Model

In the proposed anchor-free MINT algorithm the moving agents share the hypothesis regarding their positions among the neighboring agents. The movement of the agents is reflected in moving virtual anchors. In this section we describe the relations between position, movement and covariance of the agents and the corresponding VAs. For a better readability, we consider first-order reflections only, restricted to a two-dimensional floorplan. The model can be extended to higher-order reflections (cf. [3]) and three dimensions.

We describe the position and orientation of the wall segment S by the vectors $\mathbf{p}_S$ and $l_S\mathbf{e}_S$, respectively, with l_S as length and $\mathbf{e}_S$ as unit vector indicating the direction of wall segment as shown in Fig. 2. The closest distance between S and agent

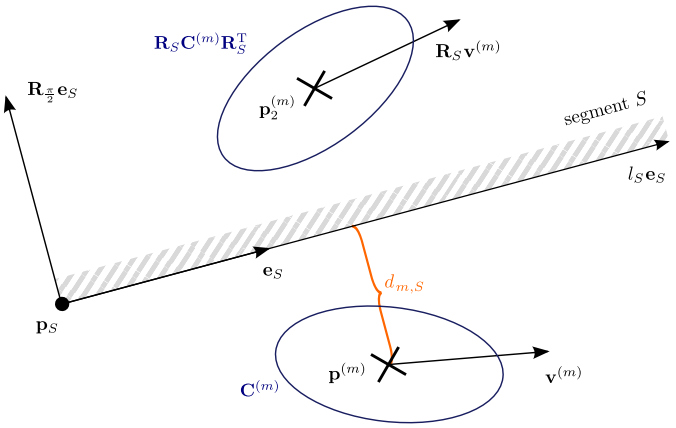

Fig. 2. Illustration of agent position $\mathbf{p}^{(m)}$, velocity $\mathbf{v}^{(m)}$ and covariance $\mathbf{C}^{(m)}$. The wall segment's orientation, indicated by $\mathbf{p}_S$ and $\mathbf{e}_S$, translates the velocity and covariance of agent m to its corresponding virtual anchors.

m is calculated by the projection of $\big(\mathbf{p}_S - \mathbf{p}^{(m)}\big)$ onto $\mathbf{R}_{\frac{\pi}{2}}\mathbf{e}_S$, where $\mathbf{R}_{\frac{\pi}{2}}$ denotes the rotation matrix by $\frac{\pi}{2}$, yielding

$$d_{m,S} = \big(\mathbf{p}_S - \mathbf{p}^{(m)}\big)^T \mathbf{R}_{\frac{\pi}{2}}\mathbf{e}_S. \tag{2}$$

The VA position $\mathbf{p}_2^{(m)}$ is calculated according to

$$\mathbf{p}_2^{(m)} = \mathbf{p}^{(m)} + 2d_{m,S}\mathbf{R}_{\frac{\pi}{2}}\mathbf{e}_S. \tag{3}$$

The motion of the agents shifts the position of the corresponding VAs, as shown in Figure 2. Agent m moves with velocity $\mathbf{v}^{(m)}$ resulting in a mirrored movement of $\mathbf{p}_2^{(m)}$ dependent on the orientation of the wall segment S. Projection of $\mathbf{v}^{(m)}$ to the orientation of S leads to the decomposition

$$\mathbf{v}^{(m)} = \big(\mathbf{e}_S^T\mathbf{v}^{(m)}\big)\mathbf{e}_S + \big(\mathbf{e}_S^T\mathbf{R}_{\frac{\pi}{2}}^T\mathbf{v}^{(m)}\big)\mathbf{R}_{\frac{\pi}{2}}\mathbf{e}_S, \tag{4}$$

where the first term on the right-hand-side represents the movement along the wall segment and the second-term the movement orthogonal to the wall segment. Mirroring of the orthogonal component and rearranging leads to the movement of the VA, given as

$$\mathbf{v}_{\mathbf{p}_2}^{(m)} = \big(\mathbf{e}_S\mathbf{e}_S^T - \mathbf{R}_{\frac{\pi}{2}}\mathbf{e}_S\mathbf{e}_S^T\mathbf{R}_{\frac{\pi}{2}}^T\big)\mathbf{v}^{(m)} = \mathbf{R}_S\mathbf{v}^{(m)}. \tag{5}$$

We denote $\mathbf{R}_S$ as VA transition matrix. It translates the movement of the agent to the movement of the corresponding

VA and depends on the orientation of the wall segment only. Further, we employ $\mathbf{R}_S$ to relate the covariance of the VAs to the covariance of the corresponding agent $\mathbf{C}^{(m)}$, as illustrated in Figure 2. Employing eigenvalue decomposition, the covariance matrix $\mathbf{C}^{(m)}$ can be represented as $\mathbf{C}^{(m)} = \mathbf{Q}\mathbf{\Lambda}\mathbf{Q}^T$ where the columns of the rotation matrix $\mathbf{Q}$ consist of the eigenvectors of $\mathbf{C}^{(m)}$ and $\mathbf{\Lambda}$ contains the eigenvalues. The covariance of the VA is expressed as follows

$$\mathbf{C}_{\mathbf{p}_2}^{(m)} = \mathbf{R}_S\mathbf{Q}\mathbf{\Lambda}\mathbf{Q}^T\mathbf{R}_S^T, \tag{6}$$

where $\mathbf{R}_S$ mirrors the eigenvectors in $\mathbf{Q}$ depending on the orientation of S.

III. Proposed Algorithm

The proposed algorithm employs at each time step n monostatic and bistatic measurements, conducted by the agents. The multipath components' delays and amplitudes of each measurement are estimated. The delays are assigned to virtual anchors to model the geometry of the MPCs. The corresponding amplitudes are used to model the uncertainty of the MPCs.

A. Channel Estimation

We use peak-picking for estimating the delays of the deterministic MPCs $\hat{\tau}_{k,n}^{(m',m)}$, implemented as an recursive least-squares approximation [8], written as

$$\hat{\tau}_{k,n}^{(m',m)} = \underset{\tau}{\operatorname{argmin}} \int_0^T |r_n^{(m',m)}(t) - \hat{r}_{k-1,n}^{(m',m)}(t) - \hat{\alpha}(\tau)s(t-\tau)|^2 dt, \tag{7}$$

with $\hat{r}_{k-1,n}^{(m',m)}(t)$ as template signal for the deterministic MPCs, estimated up to the $(k-1)$-th iteration step, and

$$\hat{\alpha}_{k,n}^{(m',m)} = \hat{\alpha}(\hat{\tau}_{k,n}^{(m',m)}), \tag{8}$$

with

$$\hat{\alpha}(\tau) = \int_0^T s^*(t-\tau)\big(r_n^{(m',m)}(t) - \hat{r}_{k-1,n}^{(m',m)}(t)\big)dt, \tag{9}$$

and T as measurement duration. The template signal $\hat{r}_{k-1,n}^{(m',m)}(t) = \sum_{k'=1}^{k-1} \hat{\alpha}_{k',n}^{(m',m)} s(t - \hat{\tau}_{k',n}^{(m',m)})$ is initialized with $\hat{r}_{0,n}^{(m',m)}(t) = 0$. Alternating between (7) and (8), the MPC parameters $\hat{\tau}_{k,n}^{(m',m)}$ and $\hat{\alpha}_{k,n}^{(m',m)}$ are recursively estimated until a predefined number $\mathring{K}_n^{(m',m)}$ is reached. The channel estimation is done for each monostatic and bistatic measurement resulting in sets of estimated distances $\mathcal{Z}_n^{(m',m)} = \big\{\hat{d}_{k,n}^{(m',m)}\big\}_{k=1}^{\mathring{K}_n^{(m',m)}}$ with $\hat{d}_{k,n}^{(m',m)} = c\hat{\tau}_{k,n}^{(m',m)}$.

B. Data Association (DA)

The estimated distances obtained from the channel estimation are now associated to expected distances calculated from VAs' positions. We calculate the set of expected distances as

$$\mathcal{D}_n^{(m',m)} = \big\{\big\|\hat{\mathbf{p}}_{1,n}^{(m')} - \hat{\mathbf{p}}_{k,n}^{(m)}\big\|\big\}_{k=1}^{K_n^{(m',m)}}, \tag{10}$$

where $\hat{\mathbf{p}}_{k,n}^{(m')}$ refers to the predicted position computed with an EKF at n. We reduce the set of expected distances to the visible ones by performing optical *ray-tracing* [19]. The number of expected distances depends on the number of segments and their visibility, and is in general different to the number of estimated MPC $\big|\mathcal{D}_n^{(m',m)}\big| = K_n^{(m',m)} \neq \big|\mathcal{Z}_n^{(m',m)}\big| = \mathring{K}_n^{(m',m)}$. We use the *optimal sub-pattern assignment* (OSPA) metric [20] to assign the expected distances to the estimated ones, where we allow a maximum discrepancy of d_c between expected and estimated distance for each MPC [8]. Finally, the assigned distances are stacked in the vector $\mathbf{z}_n^{(m',m)}$.

C. State Space and Measurement Model

We describe the state dynamics using a linear, constant-velocity motion model. In the following we describe the state vector of a single agent m. We drop the agent index m for a better readability. The joint state space of the agent and the corresponding VAs is given as

$$\tilde{\mathbf{x}}_n = [\mathbf{p}_{1,n}^T, \mathbf{v}_n^T, \mathbf{p}_{2,n}^T, \dots, \mathbf{p}_{\tilde{K}_n+1,n}^T]^T, \tag{11}$$

with $\tilde{K}_n$ denoting the number of assigned VAs at n. The state space model for one agent follows as

$$\begin{aligned}\tilde{\mathbf{x}}_n &= \underbrace{\begin{bmatrix}\mathbf{F} & \mathbf{0}_{4\times 2\tilde{K}_n} \\ \mathbf{0}_{2\tilde{K}_n\times 2} & \mathbf{I}_{2\tilde{K}_n\times 2\tilde{K}_n}\end{bmatrix}}_{\tilde{\mathbf{F}}_n} \tilde{\mathbf{x}}_{n-1} + \underbrace{\begin{bmatrix}\mathbf{G} \\ \mathbf{0}_{2\tilde{K}_n\times 2}\end{bmatrix}}_{\tilde{\mathbf{G}}_n} \mathbf{n}_{a,n}, \\ \mathbf{F} &= \begin{bmatrix}1 & 0 & \Delta T & 0 \\ 0 & 1 & 0 & \Delta T \\ 0 & 0 & 1 & 0 \\ 0 & 0 & 0 & 1\end{bmatrix} \quad \mathbf{G} = \begin{bmatrix}\frac{\Delta T^2}{2} & 0 \\ 0 & \frac{\Delta T^2}{2} \\ \Delta T & 0 \\ 0 & \Delta T\end{bmatrix},\end{aligned} \tag{12}$$

and $\mathbf{n}_{a,n}$ as zero mean driving noise.

The stacked VA transition matrix $\tilde{\mathbf{R}}_{S,n} = [\mathbf{R}_{S_2}^T, \dots, \mathbf{R}_{S_{\tilde{K}_n+1}}^T]^T$ with dimension $(2\tilde{K}_n \times 2)$ translates the movement $\mathbf{v}_n$ of the agent to the corresponding VAs. It is structured in the same manner as the stacked VAs' positions and each entry $\mathbf{R}_{S_k}$ is calculated according to (5).

The covariance of the state vector of one agent is written as

$$\tilde{\mathbf{C}}_n = \begin{bmatrix}\mathbf{C}_{\mathbf{p},n} & \mathbf{C}_{\mathbf{pv},n} & \mathbf{0}_{4\times 2\tilde{K}_n} \\ \mathbf{C}_{\mathbf{pv},n}^T & \mathbf{C}_{\mathbf{v},n} & \\ \mathbf{0}_{2\tilde{K}_n\times 4} & & \tilde{\mathbf{C}}_{S,n}\end{bmatrix}, \tag{13}$$

where $\mathbf{C}_{\mathbf{p},n}$, $\mathbf{C}_{\mathbf{v},n}$ and $\mathbf{C}_{\mathbf{pv},n}$ are the position and velocity covariance and cross-covariance matrices, respectively. The block-diagonal matrix $\tilde{\mathbf{C}}_{S,n} = \operatorname{diag}\big\{[(\mathbf{R}_{S_2}\mathbf{C}_{\mathbf{p},n}\mathbf{R}_{S_2})^T, \dots, (\mathbf{R}_{S_{\tilde{K}_n}}\mathbf{C}_{\mathbf{p},n}\mathbf{R}_{S_{\tilde{K}_n}})^T]\big\}$ with dimension $(2\tilde{K}_n \times 2\tilde{K}_n)$ aligns the covariance of the position of the agent to the VA positions, as in (6).

The individual state spaces of the cooperating agents m are stacked into a joint state space as follows

$$\underbrace{\begin{bmatrix}\tilde{\mathbf{x}}_n^{(1)} \\ \vdots \\ \tilde{\mathbf{x}}_n^{(M)}\end{bmatrix}}_{\mathbf{x}_n} = \begin{bmatrix}\tilde{\mathbf{F}}_n^{(1)} & & \mathbf{0} \\ & \ddots & \\ \mathbf{0} & & \tilde{\mathbf{F}}_n^{(M)}\end{bmatrix} \underbrace{\begin{bmatrix}\tilde{\mathbf{x}}_{n-1}^{(1)} \\ \vdots \\ \tilde{\mathbf{x}}_{n-1}^{(M)}\end{bmatrix}}_{\mathbf{x}_{n-1}} + \begin{bmatrix}\tilde{\mathbf{G}}_n^{(1)} \\ \\ \tilde{\mathbf{G}}_n^{(M)}\end{bmatrix} \mathbf{n}_{a,n}, \tag{14}$$

and $\mathbf{C}_n = \mathrm{diag}\left\{[\tilde{\mathbf{C}}_n^{(1)}, \ldots, \tilde{\mathbf{C}}_n^{(M)}]\right\}$, where we assume independent movement of the agents.

The measurement model translates the agent and VA positions to distances of the MPCs according to

$$\mathbf{z}_n = h_n(\mathbf{x}_n) + \mathbf{n}_n, \tag{15}$$

with $\mathbf{n}_n$ as zero mean measurement noise. The measured distances of the associated MPCs (see III-B) for the monostatic and bistatic measurements are stacked in $\mathbf{z}_n = [\mathbf{z}_n^{(1,1)}, \ldots, \mathbf{z}_n^{(1,M)}, \mathbf{z}_n^{(2,1)}, \ldots, \mathbf{z}_n^{(2,M)}, \ldots, \mathbf{z}_n^{(M,M)}]^T$ of length $\bar{K}_n = \sum_{m'} \sum_{m} \tilde{K}_n^{(m',m)}$. The EKF employs the Jacobian $\mathbf{H}_n$ of the non-linear measurement function $h_n(\mathbf{x}_n)$ with respect to the agent and VA positions in $\mathbf{x}_n$. It is constructed as follows: the rows in $\mathbf{H}_n$ transform the positions of one pair of a VA and an agent. For each measured distance $\bar{k} \in \{1, \bar{K}_n\}$, let m' denote the receiving agent and k the transmitting VA of agent m. Further, let μ and η be the indices locating $\mathbf{p}_{1,n}^{(m')}$ and $\mathbf{p}_{k,n}^{(m)}$ within the joint state vector. Then, the vector $\mathbf{h}_{\bar{k},n}^{(m',m)} = \left[\frac{\partial \|\mathbf{p}_{1,n}^{(m')} - \mathbf{p}_{k,n}^{(m)}\|}{\partial x_n^{(m')}}, \frac{\partial \|\mathbf{p}_{1,n}^{(m')} - \mathbf{p}_{k,n}^{(m)}\|}{\partial y_n^{(m')}}\right]$ determines the derivative of the Euclidean norm with respect to the x- and y-position coordinates of the agent and $-\mathbf{h}_{\bar{k},n}^{(m',m)}$ of the VA position where the negative sign accounts for the derivative with respect to the VA. We plug $\mathbf{h}_{\bar{k},n}^{(m',m)}$ and $-\mathbf{h}_{\bar{k},n}^{(m',m)}$ in $\mathbf{H}_n$ at row $\bar{k}_n$ and columns μ and η, respectively.

D. Range Uncertainty Estimation

The uncertainty of the measured distances $\mathrm{var}\{\hat{d}_{k,n}^{(m',m)}\}$ is related to the SINR of the corresponding delay estimate, employing the information inequality according to [8], [21]

$$\mathrm{var}\{\hat{d}_{k,n}^{(m',m)}\} \geq \left(\frac{8\pi^2\beta^2}{c^2}\mathrm{SINR}_{k,n}^{(m',m)}\right)^{-1}, \tag{16}$$

where β is the effective (root mean square) bandwidth of $s(t)$. We estimate the SINR using a method of moments estimator [8] taking the corresponding amplitudes $\{\hat{\alpha}_{k,i}^{(m',m)}\}_{i=n-N}^{n}$ over a window of N past measurements into account and compute the distance variances of each MPC according to (16).

The measurement noise covariance matrix is assembled as follows

$$\mathbf{R}_n = \mathrm{diag}\{\mathrm{var}\{\hat{d}_{k,n}^{(m',m)}\}\} \quad \forall\, m, m', k. \tag{17}$$

IV. Results

The performance of the proposed algorithm is evaluated in terms of localization error and robustness to uncertainties in the floorplan. We test the algorithm using scenarios with synthetic and measured data as explained in the following.

A. Setup for synthetic data

The setup for the synthetic scenario is as follows: a unit-energy root-raised-cosine pulse with roll-off factor of $R = 0.6$ and a pulse duration of $T_\mathrm{p} = 0.5\,\mathrm{ns}$ acts as transmit signal $s(t)$. The received signal is modeled according to (1) considering first-order reflections only. We employ a free-space propagation model attenuating the received pulses according to Friis' transmission equation. Each reflection is accounted as an additional attenuation of 3 dB. We set the parameters of the DM according to [3], where also a validation of the model is presented. The SNR between LOS (at 1 m) and additive white noise is set to 26 dB. We use $M = 3$ agents moving along the trajectories with varying velocities, shown in Figure 3. The trajectories consist of 100 position points for each agent.

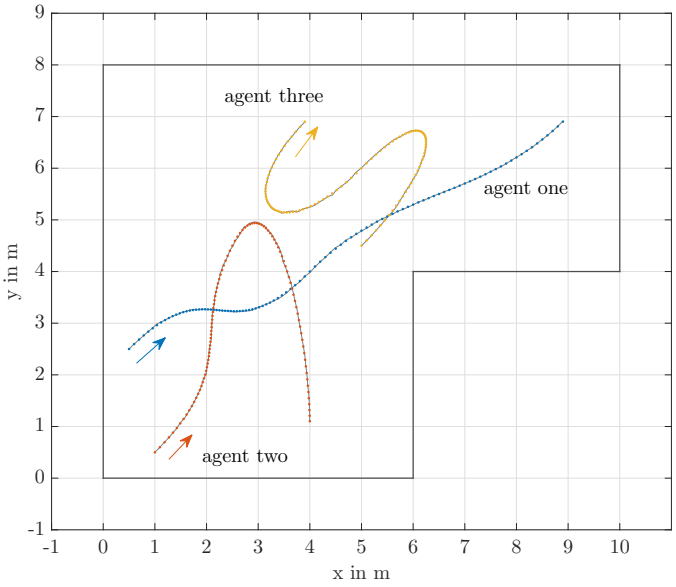

Fig. 3. Simulation scenario with synthetically generated signals: three agents move independently along the trajectories (dotted) with varying velocity.

B. Setup for measured data

The measured data are obtained using a *Rohde and Schwarz ZVA-24* VNA within a frequency range from 3.1 to 10.6 GHz. We shape the data with a root-raised-cosine pulse with roll-off factor of $R = 0.6$ and a pulse duration of $T_\mathrm{p} = 0.5\,\mathrm{ns}$ at a carrier frequency of $f_c = 7\,\mathrm{GHz}$ [22]. We use self-made Euro-cent coin antennas [23] with a uniform radiation pattern in azimuth domain. The antennas are connected to the VNA to omit the required synchronization accuracy among the agents in the order of 10^{-10} s. Figure 4 illustrates the scenario: two agents move along their trajectories consisting of 220 positions with a spacing of 5 cm. In both scenarios no anchors are used.

C. Implementation

We employ an EKF for tracking the agent states jointly with the VA states. Once a new agent joins the cooperative localization, the positions of the agents' VAs are initialized according to (3) followed by assembling the VA transitions (5). At each time step n the joint state is predicted by (14) followed by associating (see Sec. III-B) the expected MPCs with the estimated ones (Sec. III-A). Finally, the EKF update step is performed to obtain the estimated agent positions $\hat{\mathbf{p}}_n^{(m)}$.

The number of expected MPCs $K_n^{(m',m)}$ (III-B) depends on the agents' positions and the rooms' geometry. The floorplans of both scenarios are dominated by parallel walls which results in $K_n^{(m',m)} = 4$ expected MPCs in each received signal $r_n^{(m',m)}(t)$.

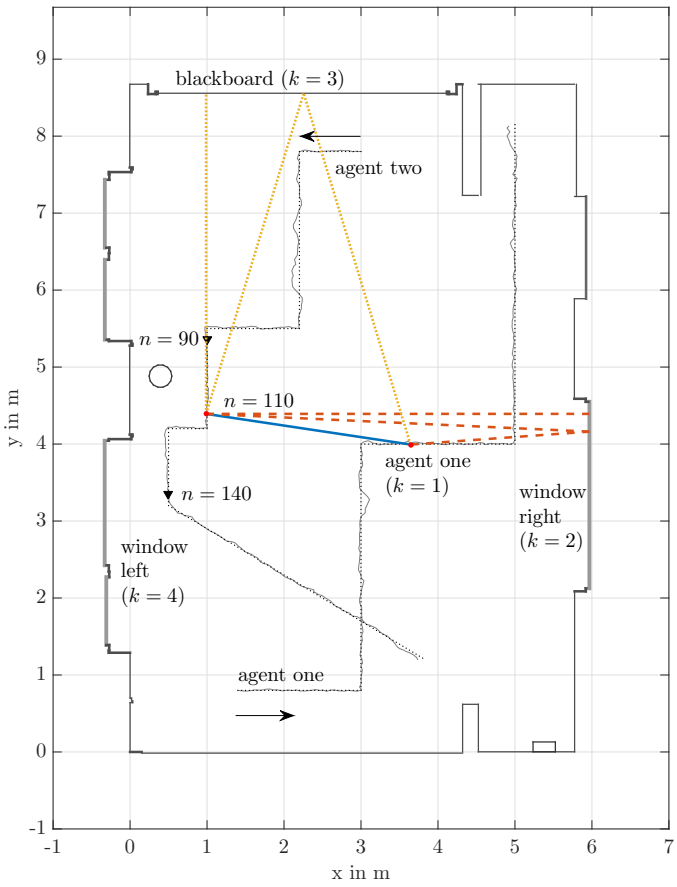

Fig. 4. Scenario with measured data obtained in the Seminar room (floorplan uncertainty $r = 1\,\text{mm}$): two agents locate their position employing MPCs along the trajectories. Multipath components are shown for time step $n = 110$.

We set the cutoff-distance in (III-B) to $d_c = cT_\text{p} = 0.15\,\text{m}$ and the number of estimated MPCs $\mathring{K}_n^{(m',m)}$ in (III-A) to $\mathring{K}_n^{(m',m)} = 1.5K_n^{(m',m)}$. Expected distance pairs within a range below the cutoff-distance of d_c are not considered in (10) for reduction of wrong data associations.

The algorithm considers past measurements received within a distance of $0.2\,\text{m}$ for MPCs' range uncertainty estimation (see Sec. III-D). The range uncertainty is used as a measure of reliability and thus gives insights on the algorithm's behavior. Figure 5 exemplifies the correspondent SINRs of selected MPCs of the measured data of agent two's trajectory from time step $n = 90$ to $n = 140$, as shown in Fig. 4. To illustrate the impact of these reflections on the task of positioning we decompose the SINR values into x- and y-components. The high SINR of the LOS between both agents ($k = 1$) indicates a low range uncertainty resulting in a strong impact on the positioning algorithm. The reflections at the right window ($k = 2$) and left window ($k = 4$) add information especially in the x-direction and the reflection at the blackboard ($k = 3$) in the y-direction. At time step $n = 120$ agent two moves behind a concrete pillar which blocks the reflection to the blackboard in the monostatic measurement. In this case, information along the y-direction is only obtained from the bistatic measurement. In general, the MPCs with index $k = \{2, 3, 4\}$ have approximately same SINRs resulting in a similar importance weight in positioning as well.

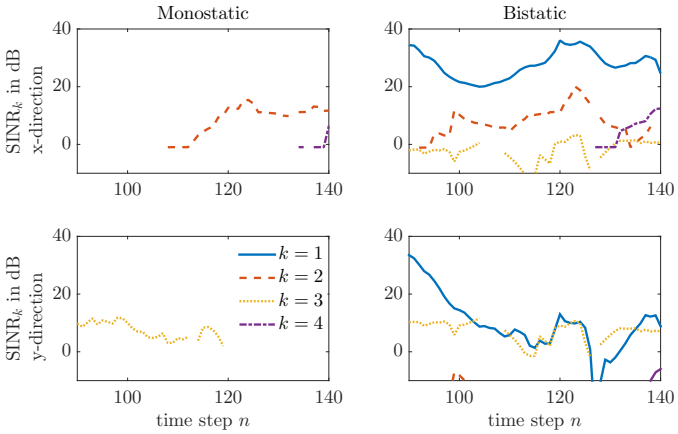

Fig. 5. SINR of LOS and multipath components along x-direction (top) and y-direction (bottom) of monostatic (left) and bistatic (right) measurements of agent two from time step $n = 90$ to $n = 140$ (see Fig. 4) of LOS ($k = 1$), window right ($k = 2$), blackboard ($k = 3$) and window left ($k = 4$).

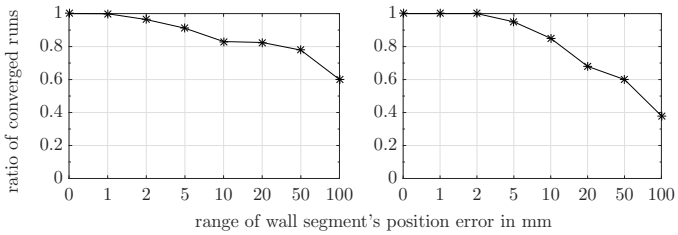

Fig. 6. Illustration of the ratio of converged runs dependent on the range of the wall segment's position error r for scenarios with synthetic (left) and measured data (right).

D. Impact of floorplan

The performance of the proposed algorithm depends on the accuracy of the provided floorplan. An imprecise floorplan leads to wrong estimates of the positions of the VAs. We examine the robustness of the algorithm when uncertainties in the floorplan are present by adding uniformly distributed noise $\mathcal{U}(-r/2, r/2)$ within the range r to the positions of the wall segments according to

$$\mathbf{p}_{S_i} = \bar{\mathbf{p}}_{S_i} + \left[\mathcal{U}(-\frac{r}{2}, \frac{r}{2}), \mathcal{U}(-\frac{r}{2}, \frac{r}{2})\right]^T, \forall i \qquad (18)$$

with $\bar{\mathbf{p}}_{S_i}$ as true position of wall segment S_i.

We perform 1000 Monte-Carlo (MC) runs with different levels of uncertainty r. We define an MC run with a maximum position error below $1\,\text{m}$ as converged. Figure 6 presents the impact of r on the ratio of converged runs. It can be seen that all MC runs converge at small wall segment position errors of $r \leq 1\,\text{mm}$. Enlarging r increases the number of outliers. The $90\,\%$ level of converged runs lies at approximately $r = 5\,\text{mm}$ for both synthetic and measured data. Figures 7 and 8 show the cumulative distribution functions (CDF) of the localization error for converged runs for the scenarios with synthetic and real measurement data, respectively. In general, the scenario

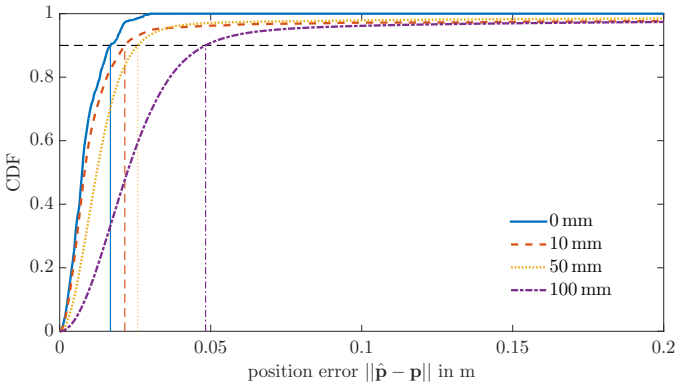

Fig. 7. CDF of the localization error for synthetic data using different ranges of wall segment errors of $r = \{0, 10, 50, 100\}$ mm for $T_\mathrm{p} = 0.5$ ns. Given a highly accurate floorplan ($r = 10$ mm) the error distance is below 25 mm in 90 % of the runs. Only converged runs are considered.

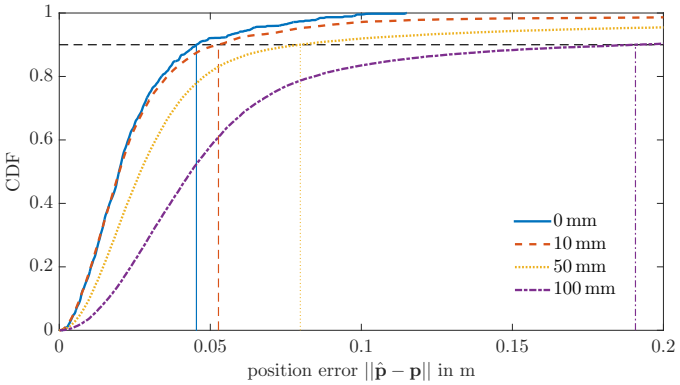

Fig. 8. CDF of the localization error for measured data using different ranges of wall segment errors of $r = \{0, 10, 50, 100\}$ mm for $T_\mathrm{p} = 0.5$ ns. Given a highly accurate floorplan ($r = 10$ mm) the error distance is below 60 mm in 90 % of the runs. Only converged runs are considered.

with synthetic data has a better performance as the synthetically generated MPCs are more stable and reliable throughout most of the scenario, compared to the real measured data. Further, the algorithm takes usage of more measurements (three monostatic and three bistatic measurements). This experiment results in an error below 25 mm in 90 % of the runs, given a highly accurate floorplan. Increasing the floorplan uncertainty up to $r = 100$ mm lowers the performance. The scenario with measured data achieves a position error of below 60 mm in 90 % of the converged runs for $r = 10$ mm. The impact of uncertainty in the floorplan is in general larger compared to the synthetic data as the reduced number of agents leads to less measurements (two monostatic and one bistatic measurement). Furthermore, the true positions of the segments $\bar{\mathbf{p}}_{S_i}$ may contain a bias due to measurement errors in the existing floorplan.

V. Conclusions

We have presented a cooperative tracking algorithm exploiting multipath propagation by using floorplan information but without fixed anchors at known locations. The performance evaluation with synthetic and measured data reveals the impact of deterministic multipath components to achieve high levels of accuracy. Given an accurate floorplan, the number of outages can be reduced to zero showing a high robustness. In future work we will further address the initialization of the joint state vector and model the floorplan's uncertainty.

References

[1] A. Conti, D. Dardari, M. Guerra, L. Mucchi, and M. Win, "Experimental Characterization of Diversity Navigation," *IEEE Systems Journal*, 2014.

[2] Y. Shen, S. Mazuelas, and M. Win, "Network Navigation: Theory and Interpretation," *IEEE J. Sel. Areas Commun.*, 2012.

[3] E. Leitinger, P. Meissner, C. Ruedisser, G. Dumphart, and K. Witrisal, "Evaluation of Position-related Information in Multipath Components for Indoor Positioning," *IEEE J. Sel. Areas Commun.*, 2015.

[4] K. Witrisal, P. Meissner, E. Leitinger, Y. Shen, C. Gustafson, F. Tufvesson, K. Haneda, D. Dardari, A. F. Molisch, A. Conti, and M. Z. Win, "High-Accuracy Localization for Assisted Living," *IEEE Signal Processing Magazine*, 2016, special Issue on Assisted Living.

[5] P. Meissner, "Multipath-Assisted Indoor Positioning," Ph.D. dissertation, Graz University of Technology, 2014.

[6] R. Parhizkar, I. Dokmanic, and M. Vetterli, "Single-channel indoor microphone localization," in *Acoustics, Speech and Signal Processing (ICASSP), 2014 IEEE International Conference on*, 2014.

[7] W. Xu, F. Quitin, M. Leng, W. P. Tay, and S. G. Razul, "Distributed localization of a RF target in NLOS environments," *IEEE J. Sel. Areas Commun.*, vol. 33, no. 7, pp. 1 – 14, Jul. 2015.

[8] P. Meissner, E. Leitinger, and K. Witrisal, "UWB for Robust Indoor Tracking: Weighting of Multipath Components for Efficient Estimation," *IEEE Wireless Communications Letters*, 2014.

[9] E. Tsalolikhin, I. Bilik, and N. Blaunstein, "A single-base-station localization approach using a statistical model of the NLOS propagation conditions in urban terrain," *Vehicular Technology, IEEE Transactions on*, vol. 60, no. 3, pp. 1124–1137, 2011.

[10] S. Van de Velde and H. Steendam, "Cupid algorithm for cooperative indoor multipath-aided localization," in *Indoor Positioning and Indoor Navigation (IPIN), IEEE International Conference on*, 2012.

[11] H. Wymeersch, J. Lien, and M. Z. Win, "Cooperative Localization in Wireless Networks," *Proceedings of the IEEE*, 2009.

[12] S. Van de Velde, H. Wymeersch, P. Meissner, K. Witrisal, and H. Steendam, "Cooperative multipath-aided indoor localization," in *IEEE Wireless Communications and Networking Conference (WCNC)*, 2012.

[13] H. Naseri, M. Costa, and V. Koivunen, "Multipath-aided cooperative network localization using convex optimization," in *Signals, Systems and Computers, 2014 48th Asilomar Conference on*, 2014.

[14] M. Froehle, E. Leitinger, P. Meissner, and K. Witrisal, "Cooperative Multipath-Assisted Indoor Navigation and Tracking (Co-MINT) Using UWB Signals," in *IEEE ICC 2013 Workshop on Advances in Network Localization and Navigation (ANLN)*, 2013.

[15] J. Kulmer, E. Leitinger, P. Meissner, and K. Witrisal, "Cooperative Multipath-assisted Navigation and Tracking: A Low-Complexity Approach," in *1st EAI International Conference on Future access enablers of ubiquitous and intelligent infrastructures, 2015*. EAI, 2015.

[16] J. B. Allen and D. A. Berkley, "Image method for efficiently simulating small-room acoustics," *The Journal of the Acoustical Society of America*, vol. 65, no. 4, pp. 943–950, 1979.

[17] K. Witrisal and P. Meissner, "Performance bounds for multipath-assisted indoor navigation and tracking (MINT)," in *IEEE International Conference on Communications (ICC)*, 2012.

[18] A. Molisch, "Ultra-Wide-Band Propagation Channels," *Proceedings of the IEEE*, 2009.

[19] ——, *Wireless communications*. John Wiley & Sons, 2007, page 132.

[20] D. Schuhmacher, B.-T. Vo, and B.-N. Vo, "A Consistent Metric for Performance Evaluation of Multi-Object Filters," *IEEE Transactions on Signal Processing*, 2008.

[21] E. Leitinger, P. Meissner, M. Lafer, and K. Witrisal, "Simultaneous Localization and Mapping using Multipath Channel Information," in *IEEE International Conference on Communications (ICC)*, 2015.

[22] P. Meissner, E. Leitinger, M. Lafer, and K. Witrisal, "MeasureMINT UWB database," 2013, Publicly available database of UWB indoor channel measurements.

[23] C. Krall, "Signal processing for ultra wideband transceivers," Ph.D. dissertation, Graz University of Technology, Austria, 2008.